Estimates of Lee-Yang zeros and a possible critical point on the pion condensate boundary in the QCD isospin phase diagram using an unbiased exponential resummation on the lattice

Sabarnya Mitra*

Centre for High Energy Physics, Indian Institute of Science Bengaluru, Bengaluru, 560012, India and Fakultät für Physik, Universität Bielefeld, D-33615 Bielefeld, Germany

(Received 14 January 2024; accepted 20 June 2025; published 18 July 2025)

Without invoking any cumulant determination at the input level, we present here the first calculations of direct estimates of the Lee-Yang zeros of the QCD partition function in $(2+1)$-flavor QCD. These zeros are obtained in the complex isospin chemical potential μ_I plane using the unbiased exponential resummation formalism on $N_\tau = 8$ lattices and with physical quark masses. For different temperatures, we illustrate the stability of the zeros closest to the origin from which we subsequently procure the radius of convergence estimates. From the temperature-dependence study of the real and imaginary parts of these zeros, we try estimating one of the possible critical points forming the second-order pion condensate critical line in the isospin phase diagram. Further, we compare these resummed estimates with the corresponding Mercer-Roberts estimates of the subsequent Taylor series expansions of the first three partition function cumulants. We also outline comparisons between resummed and Taylor series results of these cumulants for real and imaginary values of μ_I and highlight the behavior of different expansion orders within and beyond the obtained resummed estimates of the radius of convergence. We also reestablish that this resummed radius of convergence can efficiently capture the onset of the overlap problem for finite real μ_I simulations.

DOI: 10.1103/h24l-2h8j

I. INTRODUCTION

The thermodynamics of quantum chromodynamics (QCD) under extreme conditions of temperature and baryon densities governs a wide spectrum of phenomena ranging from the creation of quark-gluon plasma [1,2] in relativistic heavy-ion collision experiments [3–7] to the dense cores of neutron stars [8–10] and pion condensate formation [11], in addition to enlightening the early stages [12] of the universe and its subsequent evolution. The QCD phase diagram [13–15] and its thermodynamics in the plane of temperature T [16–18] and baryon chemical potential μ_B [19–22] are of prime relevance and utmost importance, both from theoretical [23–25] and experimental [3–5] perspectives. However, the notorious sign problem [26–28], complexifying the Monte Carlo integral measure and precluding standard importance sampling techniques, hinders any possible direct effort of mapping this phase diagram and drawing conclusive evidence from first-principle lattice QCD calculations. Despite numerous approaches [29–35] of circumventing the problem and uncovering the phase diagram, most of it is still unknown and requires further convincing results. This is one of the motivations for exploiting an alternative avenue in the direction of the isospin chemical potential $\mu_I = (\mu_u - \mu_d)$ with up- and down-quark chemical potentials μ_u, μ_d, which, unlike μ_B, introduces an asymmetry between up- and down-quark densities without introducing a sign problem. This inspires profound interest in using direct lattice QCD simulations for the purpose of exploring the resulting $T - \mu_I$ isospin phase diagram of QCD [36–40]. Besides manifesting the familiar hadronic and quark-gluon plasma phases, respectively, below and above their smooth crossover line [16,18] around $T \approx 157$ MeV at zero μ_I, the various state-of-the-art model studies also predict two other principal phases and regimes in this isospin phase diagram for low T: (i) a Bose-Einstein condensate (BEC) of charged pions for $\mu_I > m_\pi$, characterized by a second-order transition of the $O(2)$ universality class [39], and (ii) a smooth crossover from the pionic BEC state into a Bardeen-Cooper-Schrieffer (BCS) color-superconducting phase at large μ_I [36], where quark Cooper pairs form in the pseudoscalar channel [41]. While the latter is explained from perturbative arguments [42], the former is well provided by the chiral perturbation theory [43] predictions, which holds reliably in the low-energy regime of

*Contact author: smitra@physik.uni-bielefeld.de

Published by the American Physical Society under the terms of the Creative Commons Attribution 4.0 International license. Further distribution of this work must maintain attribution to the author(s) and the published article's title, journal citation, and DOI. Funded by SCOAP³.

QCD. Despite significant progress using functional methods [22], chiral effective theories [36], and both canonical [44] and grand-canonical lattice approaches, quantitative details regarding the nature and curvature of transition lines separating the relevant phases for different values of T, μ_I remain elusive and demand further study. Similarly, the perturbative predictions concerning the possible emergence of a first-order transition at asymptotically large values of μ_I accompanied by decoupling of the gluon sector also remain under active investigation.

In this work, the central focus is on the pion phase boundary that separates the pion condensate phase from the hadronic noncondensate phase. At low temperatures and small values of μ_I, the phase diagram is characterized by the formation of a pion condensate. As μ_I increases, the energy required to create charged pions is reduced due to their coupling to the isospin chemical potential μ_I. When μ_I reaches the critical value $\mu_{I,c}$, it becomes energetically favorable for charged pions to condense into a Bose-Einstein-like ground state. With this value of $\mu_{I,c}$ depending on the initial choice of convention of the theory, current studies in the literature toggle between $\mu_{I,c} = m_\pi$ [36] and $m_\pi/2$ [39] for $T = 0$ in the phase diagram, where the transition into the pion condensed phase across the pion phase boundary line is a second-order phase transition characterized by a nonzero expectation value of the charged pion field $\langle \pi^{\pm} \rangle$ and the spontaneous breaking of the residual $U(1)$ isospin symmetry, accompanied by the presence of a Goldstone mode. This transition occurs primarily at low temperatures, where there are less thermal fluctuations, which are insufficient to disrupt the coherence of the condensate. While chiral perturbation theory (χPT), which is reliable in the regime of small T, μ_I, predicts a monotonic slope of this critical line with an increasing value of critical μ_I for rising T, recent studies [39] have found that this line remains vertical in the $T - \mu_I$ plane up to $T \approx 140$ MeV starting from $\mu_{I,c} = m_\pi/2$ (m_π here and also in Refs. [36,38]) at $T = 0$, before the thermal effect starts dominating for higher temperatures and thereby melting the condensate close to and beyond the crossover temperature $T \approx 157$ MeV. Further studies are required for a firmer statement regarding the thermal nature of this pion condensate critical line.

In the present work, we leverage the recently developed method of unbiased exponential resummation [35,45] for probing the analytic structure of the isospin partition function in the complex μ_I plane without introducing any form of pionic regulator in the working QCD action, where the central goal is to have an understanding of the QCD isospin phase diagram in the low T, small μ_I regime from the perspective of Lee-Yang zeros and the related nonanalytic structure of the isospin partition function. By obtaining and locating the Lee-Yang zeros of the partition function in its polynomial form in the complex μ_I plane using the Newton-Raphson method, we procure a nonperturbative resummed estimate of the radius of convergence by determining the closest Lee-Yang zero from the origin and evaluating its distance from the origin. As outlined in detail in this paper, we also verify the stability of these zeros, which, as we will observe, subsequently yields encouraging indications. This is promising, as these zeros and the associated radius of convergence offer valuable insights regarding the proximity of possible phase transitions in μ_I although, strictly speaking, one needs to investigate these zeros in the thermodynamic limit for confirming possible phase transitions or crossovers. With information from the study of the temperature dependence of the radius of convergence estimates and the same for the imaginary parts of the nearest complex Lee-Yang zeros, we procure a quantitative measurement of the estimate of a true critical point in the isospin phase diagram. In Sec. VI, we show and discuss that this critical point, obtained for the first time in this manner, happens to lie on the second-order pion phase boundary critical line within the respective error bars for the respective T and μ_I values. This agreement is consistent with the starting convention of this work, which otherwise influences the critical $\mu_{I,c}$ marking the onset of the pion phase. Although this has no implication on the order and universality class of this phase transition, observing the critical point on the pion phase boundary from a direct Lee-Yang zero analysis at this low temperature is a novel feature of this work; additionally, this is achieved without relying on the knowledge of the partition function cumulants, which is unlike previous works [46–49] in the prevailing lattice QCD literature on Lee-Yang zero [50] analysis and determination. Through this work and its pertinent study, we strive toward attaining a quantitative characterization of the QCD isospin phase diagram. This attempt will not only refine our existing knowledge of pion condensation at finite isospin density from the new unbiased resummation approach, but it will also pave the way in the future for similar studies and related insights for the more experimentally relevant finite baryon densities. Besides comparing this resummed estimate of the radius of convergence with the corresponding Mercer-Roberts (MR) [51–53] estimates of that obtained from the Taylor expansion series, we also illustrate the comparison between the resummed and the Taylor series results of various order cumulants and outline the behavior of different orders within and beyond this unbiased resummed estimate of the radius of convergence for several working temperatures presented in this paper. This has been shown here using an eighth order Taylor expansion around $\mu_I = 0$ for the first three cumulants of the partition function [54–57]. To summarize in brief, the flow of the work presented here is as follows: (1) computing the nearest Lee-Yang zeros on lattices with physical quark masses using the Newton-Raphson algorithm in the complex μ_I plane, (2) tracking the temperature dependence of their real and imaginary parts to gauge the possible critical point, and

(3) benchmarking the resummed convergence radii against the stable Mercer-Roberts estimators derived from high-order Taylor coefficients. Toward the end of this paper, we also briefly outline the onset of the overlap problem across the obtained resummed radius.

The paper is organized as follows: In Sec. II, we review the formalism of finite-density Taylor series expansions by introducing the QCD partition function. We also briefly outline the unbiased exponential resummation method and the Newton-Raphson procedure, both of which form a central part of this work and have been implemented at length in this paper. Although well known, we summarize these methods and introduce the basic notations, which we extensively use here to estimate the respective Lee-Yang zeros. Section III details our lattice setup and the related simulation parameters of the results presented in this paper. In this section, we also illustrate the relevant quark and pion quantum numbers that influence the onset point of the pion condensate in the phase diagram. From Sec. IV onwards, we demonstrate the central results of this work in μ_I with clear arguments. Instrumental to the work here, this core section is devoted to the computation and analysis of Lee-Yang zeros in the complex μ_I plane described in Sec. IV A, including a detailed discussion in Sec. IV B on their stability and extent of reliability for extracting meaningful results and subsequent conclusions. As we will observe, the Lee-Yang zero situated nearest to the origin yields maximal relevance since it gives the estimate of the resummed radius of convergence, which is subsequently mapped to the possible determination of the critical point and phase boundary. Section V discusses the temperature dependence of the real and imaginary parts of this closest Lee-Yang zero for different working temperatures. From these data, the linear extrapolation toward a possible critical point at some critical T and μ_I is performed, which is clearly mentioned and presented in Sec. VI A, where the radius of convergence estimates for various temperatures are also highlighted. Besides demonstrating the measure of the critical point and its location on the pion phase critical line, we also illustrate comparisons between this resummed estimate of the radius of convergence and the Mercer-Roberts measures of the same, as shown in Sec. VI B. The latter two estimates are obtained from Taylor series results. These results have been obtained using the recent HotQCD data with more improved statistics for $N_\tau = 8$ lattices [58]. We also extend this comparative study to the level of individual cumulants of the partition function in Sec. VI C, where we observe order-by-order disagreement beyond this resummed radius of convergence. Following this, we discuss the overlap problem in Sec. VII and conclude in Sec. VIII with an outlook on possible future extensions. In the Appendix, we discuss the choice and reasoning of our starting isospin convention and the subsequent relevant quantum numbers of u, d quarks and pions. Throughout this paper, we have used relativistic units and the Boltzmann constant. Except in Sec. II A, we use μ_B and μ_I to denote μ_B/T and μ_I/T in this paper.

II. ESSENTIAL NOTATIONS AND FORMULAS

In this section, we introduce some basic notations and revisit some well-known formulas which we use in this paper.

A. Taylor expansion and unbiased exponential resummation

For $(2+1)$-flavor QCD with gluons described by a Symanzik-improved [59] gauge action S_g and quarks described by the highly improved staggered quark (HISQ) action [60–62], the grand-canonical partition function $\mathcal{Z}(\mu, T)$ in the thermodynamic limit for a temperature T and chemical potential μ is represented by

$$\mathcal{Z}(T,\mu) = \int \mathcal{D}U e^{-S_g[U(T)]} [\det \mathcal{M}(\mu, T, U)]^{1/4} \quad (1)$$

with the Euclidean gauge action S_g and the fermion matrix $\mathcal{M}$. This partition function is important for constructing the different-order μ cumulants useful for knowing finite-density QCD thermodynamics. The finite μ Taylor expansion of the QCD excess pressure yields an even series in μ owing to the particle-antiparticle symmetry of QCD. Up to $\mathcal{O}(\mu^N)$, this is given by

$$\frac{\Delta P_N^{\mathrm{T}}}{T^4} = \sum_{n=1}^{N/2} \frac{\mathcal{X}_{2n}}{(2n)!} \left(\frac{\mu}{T}\right)^{2n} \quad (2)$$

where, in Eq. (2), ΔP_N^{T} is the Taylor estimate of excess pressure $\Delta P(\mu)$ defined as $\Delta P(\mu) = P(\mu) - P(0)$, and the Taylor coefficients $c_{2n} = \chi_{2n}/(2n)!$

Unlike the Taylor expansion, the unbiased exponential resummation starts its approximation from the level of $\mathcal{Z}$ and harnesses an estimate of $\Delta P(\mu)$ comprising a series to all orders in μ. This is given by

$$\frac{\Delta P_N^{\mathrm{R}}}{T^4} = \frac{1}{VT^3} \ln \left[\frac{\mathcal{Z}(\mu)}{\mathcal{Z}(0)}\right]_{\mathrm{R}}, \quad \text{where}$$
$$\left[\frac{\mathcal{Z}(\mu)}{\mathcal{Z}(0)}\right]_{\mathrm{R}} = \langle e^{A_N(\mu)} \rangle \quad \text{with}$$
$$A_N(\mu) = \sum_{n=1}^{N} \frac{\mathcal{C}_n}{n!} \left(\frac{\mu}{T}\right)^n. \quad (3)$$

These coefficients C_n in Eq. (3) are constructed from different linear combinations of the various n-point correlation functions D_n. An elaborate study of this case with mathematical details is given in [35,45], whereas unbiased estimates and their importance are given in [63–65]. For a given order n, we have seen that this formalism yields

identical Taylor coefficients of each order $\leq n$, as well as provides nonzero estimates for all the higher orders. We will extensively use this method of resummation for all our work presented in this paper.

B. Newton-Raphson method

By using the unbiased exponential resummation to approximate the partition function $\mathcal{Z}(\mu)$ from its path integral form, we explicitly make use of the Newton-Raphson method to numerically evaluate the Lee-Yang zeros of this $\mathcal{Z}$, as a function of μ_I. Starting from an initial guess μ_0, one converges toward the actual analytic root of the function $f(\mu) \equiv [\mathcal{Z}(\mu)$ in our work] through several iterations following the recursive relation

$$\mu_{n+1} = \mu_n - \frac{f(\mu_n)}{f'(\mu_n)}. \tag{4}$$

Here, $f'(\mu_n)$ indicates the first derivative of f with respect to μ at $\mu = \mu_n$, the value of the root at the nth iteration. The algorithm is designed so that these iterations continue until a maximum allowed value N_U and values of μ_{n+1} are generated sequentially, unless $|\mu_{n+1} - \mu_n| \leq \epsilon$, where ϵ is the tolerance limit value of the given Newton-Raphson method. The values of the initial guess μ_0 and the tolerance ϵ determine the pace of convergence of this method [66]. One keeps the upper limit N_U of these iterations sufficiently high so that the target tolerance is reached, ensuring the algorithm never fails to attain the root value for given μ_0 and ϵ, for $1 \leq n \leq N_U$, as per Eq. (4).

III. SETUP OF LATTICE AND SIMULATIONS

For the analysis presented in this paper, we have used the data generated by the HotQCD Collaboration for its ongoing Taylor expansion calculations of the finite-density QCD equation of state, chiral crossover temperature, and conserved charge cumulants at finite density [67–71]. A detailed overview and description of the gauge ensembles and scale setting can be found in Ref. [69]. In these HotQCD data, $(2+1)$-flavor gauge configurations are generated in the temperature range $T \in [125:176]$ MeV using a Symanzik-improved gauge action and a HISQ fermion action on different size lattices. The temperature for each N_τ is tuned by varying the lattice spacing a through the gauge coupling β; also for each lattice spacing, the bare light and strange quark masses $m_l(a)$ and $m_s(a)$ are tuned so that the pseudo-Goldstone pion and kaon masses remain equal to the physical pion and kaon masses, respectively. This scale illustrating the important line of constant physics [17,72] has been determined using the Sommer parameter r_1 as well as the kaon decay constant f_K, in which the quark masses are procured from the former scale while the latter is used for obtaining the temperature values already quoted in this paper. Here, we work on $32^3 \times 8$ lattices with physical values of bare quark masses in $2+1$-flavor QCD, in which $m_l = m_s/27$. In order to calculate the n-point correlation functions D_n and different-order Taylor coefficients for each of our working temperatures, the first eight derivatives $D_1^f, \ldots, D_8^f$ for each quark flavor $f = u, d, s$ are estimated stochastically using 500 Gaussian random volume sources on every working gauge configuration, from which the μ_I derivatives were obtained.

For this work, we have considered the isospin quantum numbers of u, d quarks as $I_u = I_d = 1/2$, resulting in the pion quantum number $I_\pi = 1$. This subsequently gives the relation $\mu_I = (\mu_u - \mu_d)$ in our working baryon, strangeness, isospin (B, S, I) basis. A detailed derivation of this case is presented in the Appendix. It leads to zero isospin correlation functions D_n^I for all odd n, and real D_n^I for even n, because of which, one finds no sign problem in lattice QCD simulations for finite real μ_I. Importantly, this starting convention choice of the quantum numbers fixes the onset of pion condensation at $\mu_I = m_\pi$, as also shown explicitly in Ref. [38]. This is unlike the same case observed at $m_\pi/2$ in the work in [39], where $I_u = I_d = 1$ and $I_\pi = 2$ have been used. Using these data and considering 20 K statistics for every temperature, we perform our calculations of the cumulants and the Lee-Yang zeros of the isospin partition function, which constitute a central part of this paper. We demonstrate these results in the next section.

IV. LEE-YANG ZEROS OF THE ISOSPIN PARTITION FUNCTION

A. Observations and results

From this point forward, we focus entirely on the isospin chemical potential μ_I. We first compute the Lee-Yang zeros $\mu_I^{\rm LY}$ of the QCD partition function $\mathcal{Z}$ in the complex μ_I plane and present these results in Fig. 1. As already mentioned, this $\mathcal{Z}$ is derived by approximating the exact path integral into a polynomial form using the unbiased exponential resummation formalism. We compute these complex roots $\mu_I^{\rm LY}$ of $\mathcal{Z}$ for different temperatures $T \in [125:171]$ MeV using the standard Newton-Raphson approach [66], where the initial guesses of the roots are constructed considering $0 \leq {\rm Re}(\mu_I), {\rm Im}(\mu_I) \leq 2.1$. This choice is based on the resulting observation, where we find that the different-order Taylor and resummed series of the cumulants of $\mathcal{Z}$ start to deviate from each other at $|\mu_I| \approx 1$, leading us to suspect that one may possibly encounter these zeros close to and beyond $|\mu_I| \approx 1$ in the complex μ_I plane. This is also related to our interest in finding the radius of convergence, which is the distance of the nearest Lee-Yang zero from the origin. In addition, with this initial choice of complex μ_I range, we try to ensure that the guess values are not too different from the actual analytic roots, which is important to sustain the validity of the Newton-Raphson approximation used in this work. Here, the zeros are computed with an error tolerance value

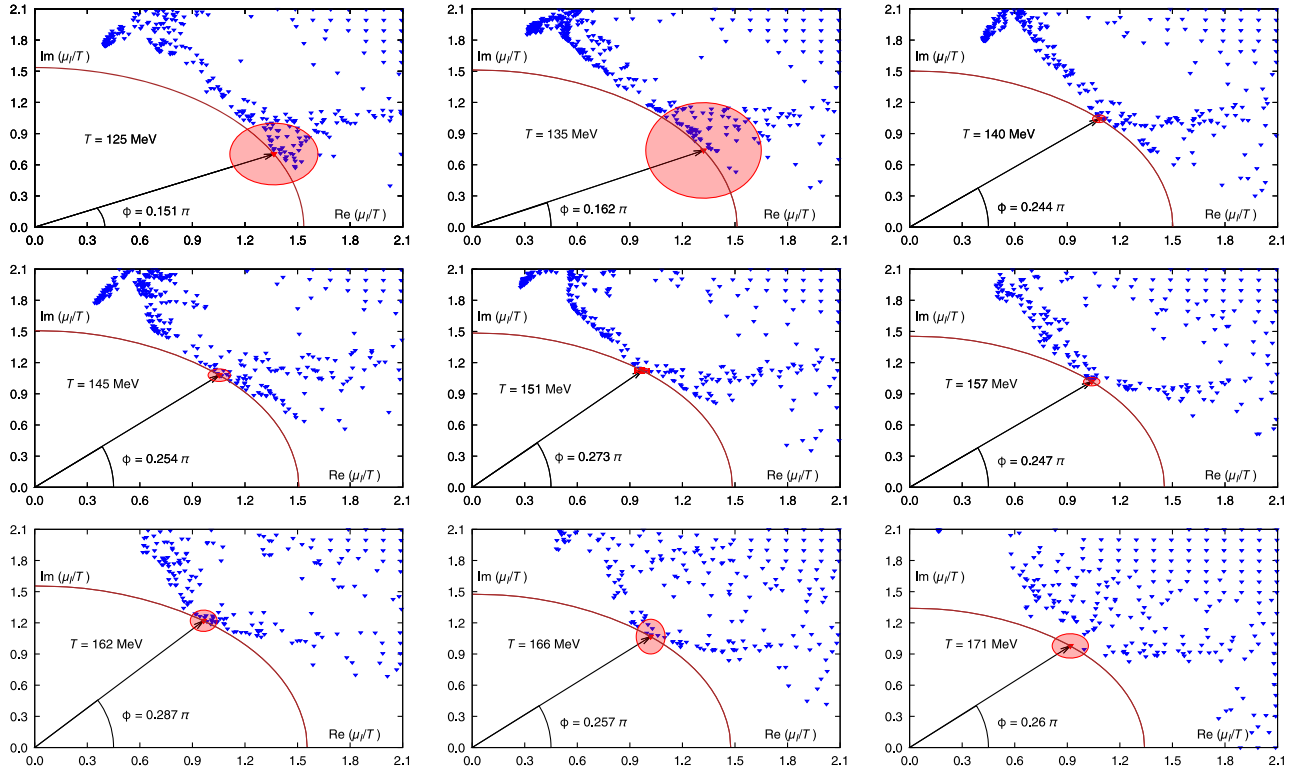


FIG. 1. Unbiased resummed estimates of the Lee-Yang zeros in the complex μ_I plane (in blue) for $125 \leq T \leq 171$ (in MeV), making different angles ϕ at the origin. The zeros closest to the origin are shown for each T, with correlated errors along real and imaginary parts accounted for by respective ellipses (in red). The brown lines show the circle of convergence in the first quadrant.

of $\epsilon = 0.002$, with the upper bound N_U on iterations kept sufficiently high, $\sim\mathcal{O}(10^8)$. Obtained through repetitive trial and error methods, this large value of N_U ensures that the algorithm does not fail and, as mentioned in Sec. II B, that it performs all the necessary required iterations and evaluates x_n and x_{n+1}, satisfying $|x_{n+1} - x_n| \leq \epsilon$. One can vary this tolerance value ϵ and observe if further smaller values ensure better results of $\mu_I^{\rm LY}$ and offer better indications of the pion phase boundary and other aspects of the QCD isospin phase diagram. However, one should also note that the number of iterations increases and so does the subsequent time for convergence. Therefore, the upper bound value N_U also requires attention and possibly further increments to avert any possible lack of convergence of this algorithm.

These complex roots are obtained after being averaged over $N_B = 100$ samples, in each of which we bootstrap the original gauge ensemble using different random seed values and thereupon evaluate these roots in the new bootstrapped gauge ensemble. With a total of 20 K configurations analyzed in each such sample, this also allows one to calculate the respective errors in the real and imaginary part measurements of these zeros. In this work, we perform and illustrate this only for the respective closest zeros μ_I^0 in Fig. 1 by constructing ellipses for different T, considering the correlations between the error bars along the real $\mu_{I,r}^0 = \mathrm{Re}[\mu_I^0]$ and imaginary parts $\mu_{I,i}^0 = \mathrm{Im}[\mu_I^0]$, respectively. In this figure, we also construct the angle ϕ made at the origin by the complex zero μ_I^0 for each working temperature. This is given by

$$\phi = \tan^{-1}\left[\frac{\mu_{I,i}^0}{\mu_{I,r}^0}\right] \tag{5}$$

where $\phi \in [0 : \pi/2]$ is ensured by the particle-antiparticle symmetry of QCD. Figure 1 clearly illustrates that μ_I^0 approaches the real μ_I axis as T is lowered, especially in the QCD hadronic regime for $T < T_{cr} \sim 157$ MeV. Except for 162 MeV, we notice a similar behavior of μ_I^0 for the high T plasma regime. This is well indicated by the ϕ values decreasing with decreasing temperature in both the QCD phases on either side of the crossover temperature T_{cr}. We also notice that, with increasing T values, the rectangular grid of blue points initially starting from the top right corner of the plots continues to become enhanced and enlarged, resulting in a larger density of zeros in the plots. This is obvious, as the Newton-Raphson method fails to converge due to very large values of the exponentially resummed $\mathcal{Z}$. This manifests in the regime of large complex μ_I values as well as for higher values of T, where the n-point correlation functions increase, resulting in a loss of convergence within

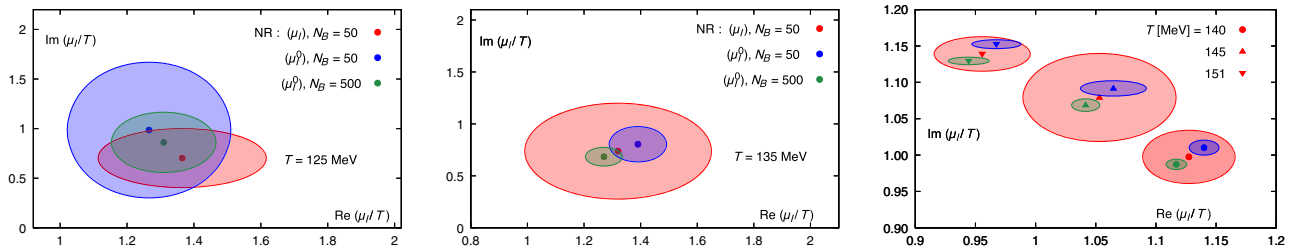


FIG. 2. Estimates of the Lee-Yang zeros in complex μ_I/T plane computed using the Newton-Raphson method are shown in red, blue and orange points respectively for $T = 125$ MeV (left) and 135 MeV (center). See full text for details. (Right) The same plot now for all the other three temperatures, $140 \leq T \leq 151$ MeV in the hadronic regime.

a few iterations; hence, the obtained estimated value is not far from the initial guess value μ_0 in the complex μ_I plane.

Interestingly, we also find from Fig. 1 that the resummed radius of convergence, $\rho_R = |\mu_I^0|$, remains close to 1.5 within error bars, which we discuss in Sec. VI. Defined as $\rho_R = \mu_I^\rho/T$, this suggests that μ_I^ρ should show a monotonic behavior in T, possibly in a linear manner in this regime. With μ_I^ρ coinciding with the pion phase boundary in the isospin phase diagram shown before in [73], this observation otherwise goes well with the predictions of χPT [36], stating a similar monotonic behavior of $\mu_{I,c} \sim \mu_I^\rho$ with T in this regime, where $\mu_I \ll m_\rho$ [74], ensuring the validity of χPT. However, before confirming these results and drawing possible conclusions, it is important to check the stability of the algorithm and the reliability of these calculated Lee-Yang zeros, which we discuss in the following section.

B. Stability of the results

In this section, we comprehensively check the stability of the closest Lee-Yang zero estimates, which we have illustrated in the previous section and also shown in Fig. 1. We consider these estimated zeros in Fig. 1 at different T as our initial guesses and subsequently implement the Newton-Raphson algorithm on these respective zeros for different temperatures. The consequent results are outlined in Fig. 2. With these new starting points μ_0 along with the same values of tolerance ϵ and maximum number N_U of allowed iterations as before, we use the Newton-Raphson method and recalculate using the identical number of bootstrap samples N_B in order to check if the algorithm manages to converge and identify these zeros efficiently. In Fig. 2, we clearly observe that for all five working temperatures, $125 \leq T \leq 151$ MeV, the final estimates of the zeros agree considerably well with the starting zero estimates within respective error bars. We also show a zoomed-in version of these results for the lowest two working temperatures at $T = 125$ and 135 MeV in Fig. 2. These figures illustrate that this agreement holds true even when the bootstrap samples N_B are increased by an order from 50 to 500, even though one can also observe that the errors decrease for the latter with higher $N_B = 500$, as shown by the green elliptical regions in Fig. 2.

In addition, we also perform an extension of this study by making use of the known critical points at 135 MeV and thereupon implementing our working Newton-Raphson method for the purpose of cross-checking the reliability of our calculated Lee-Yang zeros, as shown in Fig. 1. The results of this stability check are presented in Fig. 3. The complex critical points $\mu_{I,c}$, as the corresponding starting guesses used in this section, have been constructed parametrically using the following:

$$\mathrm{Re}(\mu_{I,c}) = m_\pi \cos\phi, \qquad \mathrm{Im}(\mu_{I,c}) = m_\pi \sin\phi \tag{6}$$

where ϕ is given in Eq. (5), and $\mu_I = m_\pi$ is the onset point of the pion condensation based on the starting convention of this work, as also used and outlined in [38]. The choice of $T = 135$ MeV is motivated by [39], where the pion condensation line is predicted at $\mu_I = m_\pi/2$ for $T \leq 140$ MeV. It must be noted that the factor of $1/2$ in [39] arises purely due to a different starting convention and, therefore, also differs from other related works [36,38]. These works not only obtain the onset at $\mu_I = m_\pi$ using chiral perturbation theory but also use the same convention as used in the present work. A relevant discussion about this is given in the Appendix.

In this section, we consider seven critical points satisfying Eq. (6), outlined as red points in Fig. 3. These correspond to seven values of ϕ, namely, $\phi = n\pi/12$ with

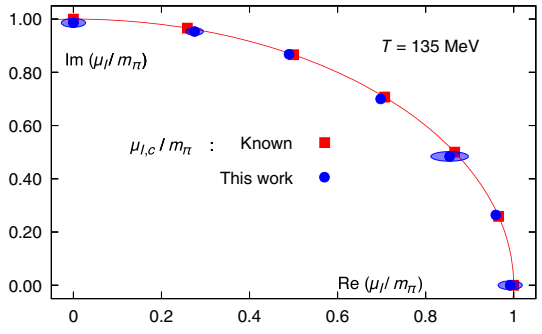


FIG. 3. Estimates of Lee-Yang zeros at $T = 135$ MeV, when one considers the values of complex μ_I satisfying $|\mu_I| = m_\pi$ as initial guesses. The red and blue points, respectively, showcase the initial guess values and the final Newton-Raphson estimates obtained with these initial guess values. Refer to text for details.

integer n satisfying $0 \leq n \leq 6$. In Fig. 3 (blue points and ellipses), we observe that the final zero estimates, obtained as a result of using the Newton-Raphson method on the red points as initial guesses, agree appreciably well within errors and converge commendably with these red points. Although interesting future works would involve improvement in the accuracy and precision of this agreement, as well as associated manifestations for smaller tolerance values, we believe that the present level of agreement achieved is appreciable and reliable enough for the current paradigm of this work.

V. REAL AND IMAGINARY PARTS OF LEE-YANG ZEROS

We explore the real and imaginary parts of these zeros separately and probe their behavior as a function of temperature. Even though we also evaluate these zeros for higher temperatures in the so-called quark-gluon plasma regime above $T_{cr} \sim 157$ MeV, we mostly concentrate on the lower temperatures in the hadronic regime, primarily because of our interest in knowing the behavior of these zeros for lower temperatures toward $T = 0$ and eventually aiming to map a critical point on the pion phase critical line in the low T, small μ_I regime of the QCD isospin phase diagram.

Having verified the reliability of the current mathematical setup for this work, we turn our attention toward the temperature-dependent behavior of the real and imaginary parts of nearest Lee-Yang zeros μ_I^0, namely, $\mu_{I,r}^0$ and $\mu_{I,i}^0$ in the complex μ_I plane. These are demonstrated in Fig. 4. One clearly observes a finite value of $\mu_{I,i}^T$ in this figure even at the lowest working $T = 125$ MeV, where $\mu_{I,i}^T$ is given as $\mu_{I,i}^T = \mu_{I,i}^0 \cdot T$. This is not surprising, as it is a natural expectation in a finite volume. However, strictly speaking, one needs to approach the thermodynamic limit in this regard, which means to check if this value of $\mu_{I,i}^T$ remains finite or if it vanishes in this limit. While the former would indicate a genuine crossover, the latter would imply a true phase transition at this temperature; hence, it is an interesting prospect to explore in the future. In Fig. 4, we find that $\mu_{I,i}^0$ reduces monotonically with decreasing temperature T at least in the low T hadronic regime below $T_{cr} \approx 157$ MeV. In addition, one also observes that the associated error bars of these $\mu_{I,i}^T$ values increase with similar statistics for $T \leq 135$ MeV, which can possibly indicate the existence of the pion condensate phase and related enhancement of fluctuations among the $\mu_{I,r}^T, \mu_{I,i}^T$ values across different bootstrap samples. One needs to perform further cross-checks and also explore other associated relevant observables for a firmer and conclusive statement in this regard. We also observe in Fig. 4 that the leading Lee-Yang zero exhibits a small yet finite imaginary part across the explored temperature range. While this observation, especially for $T \leq 140$ MeV in this figure, may seem at odds with the usual,

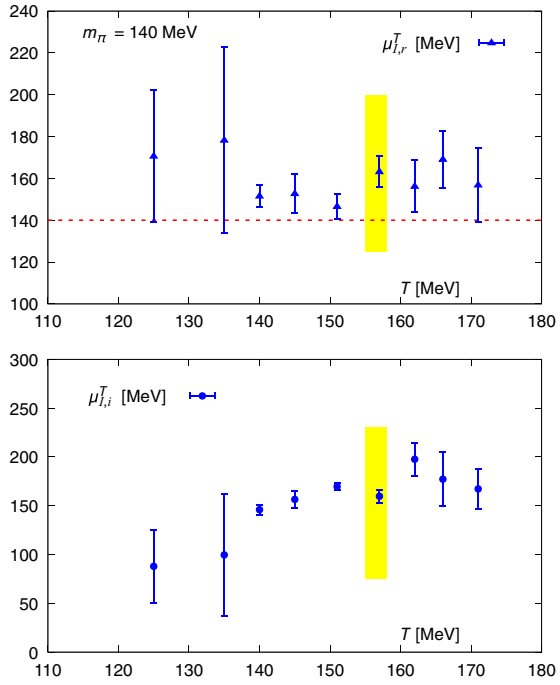


FIG. 4. Real part $\mu_{I,r}^T = \mathrm{Re}[\mu_I^0] \cdot T$ (top) and the imaginary part $\mu_{I,i}^T = \mathrm{Im}[\mu_I^0] \cdot T$ (bottom) as a function of temperature T for $125 \leq T \leq 171$ MeV with error bars. The red dotted line in the top figure marks the value of the physical $m_\pi = 140$ MeV. The yellow band shows the crossover region $T_{cr} = 156.5(1.5)$ MeV, as obtained from [15].

prevailing expectation of a real zero for a genuine second-order phase transition in the thermodynamic limit as provided by the current state-of-the-art studies [39], we interpret this feature as a combined outcome of finite-volume effects and possible artifacts of the working method of unbiased exponential resummation in the present work. With the belief that a comprehensive finite-size scaling analysis of these zeros and their behavior in the thermodynamic limit would explain these nonvanishing $\mu_{I,i}^0$ and possibly mitigate them for $T \leq 140$ MeV, we leave a detailed discussion of these various artifacts and corrections for future work.

Apart from the behavior of the imaginary part $\mu_{I,i}^T$, Fig. 4 also demonstrates the T dependence of the real part $\mu_{I,r}^0$ or, equivalently, $\mu_{I,r}^T = \mu_{I,r}^0 \cdot T$. Unlike $\mu_{I,i}^T$, in this case, one observes that $\mu_{I,r}^T$ qualitatively exhibits a fluctuating yet saturation-like behavior, with no indications of any sort of strict monotonic reduction or increment like $\mu_{I,i}^T$. Interestingly, in this case, we find that—at least for lower $T \leq 135$ MeV, i.e., at $T = 125, 135$ MeV—$\mu_{I,r}^T$ shows good agreement within error bars with $\mu_{I,r} = m_\pi = 140$ MeV, which also marks the value of the physical pion mass used in this work. This is depicted in Fig. 4 by the red dotted line. Besides these two temperatures, the behavior of $\mu_{I,r}^T$ for other temperatures, also in the hadronic regime for $140 \leq T \leq 151$ MeV in Fig. 4, clearly manifests values which remain quantitatively close to 140 MeV and therefore do not differ

too much from the red dotted line. We reserve discussions of the high T regime for future work.

The joint behavior of $\mu^T_{I,r}$ and $\mu^T_{I,i}$ for the lower $T \leq 135$ MeV shows consistency with the present idea outlined in [73], where it is argued that the radius of convergence μ^ρ_I for a finite volume at large enough orders satisfies

$$\mu^\rho_I \approx \sqrt{(\mu_{I,p})^2 + (\mu^T_{I,i})^2}, \tag{7}$$

with $\mu^T_{I,i}$ the imaginary part of the closest complex Lee-Yang zero and $\mu_{I,p}$ the phase transition chemical potential value in the infinite-volume thermodynamic limit. This implies that the real part $\mu^T_{I,r}$ approximately saturates toward the expected true phase transition $\mu_{I,p}$ even at finite volume for low enough temperatures, where one expects the imaginary part $\mu^T_{I,i}$ to be nonvanishing and finite and showing some temperature-dependent behavior. We observe both of these manifestations from Fig. 4 within error bars, where there is a monotonic reduction with decreasing T in the imaginary sector, and the real parts seem to saturate toward the physical pion mass value 140 MeV, shown by the red dotted line. Consequently, the failure of the radius of convergence estimate μ^ρ_I in Eq. (7) to converge at the true critical point in finite-volume simulations for these temperatures is mostly attributed to the nonvanishing value of the imaginary part $\mu^T_{I,i}$ of the Lee-Yang zero μ^0_I, which may possibly vanish in thermodynamic limit if the phase transition is genuine for this range of temperatures. We leave this analysis for future work.

In line with [73] and also as evidence of the onset of the pion condensate phase at $\mu_I = m_\pi$, in Fig. 5 we outline the isospin susceptibility χ_n behavior for different orders n at $T = 135$ MeV as a function of μ_I/m_π with $m_\pi = 140$ MeV. This is to obtain a possible set of observations from the perspective of reweighting via the unbiased exponential resummation approach. The isospin susceptibility $\chi = \partial\mathcal{N}/\partial\mu_I$ is chosen, as it is roughly the number-density–to–chemical-potential ratio probed in [73]. Figure 5 clearly illustrates that, starting from $\mu_I = m_\pi$, the sixth order reweighted isospin susceptibility χ^R_6 obtained via the unbiased exponential resummation method (shown as red points) deviates sharply from the same susceptibility obtained from different-order Taylor series χ^T_n (shown as bands in this figure). This is encouraging, as it offers manifestations similar to what has also been observed in [73] and thus provides promising indications about the possible existence of the pion condensation phase boundary at $\mu_I = m_\pi$ for this temperature.

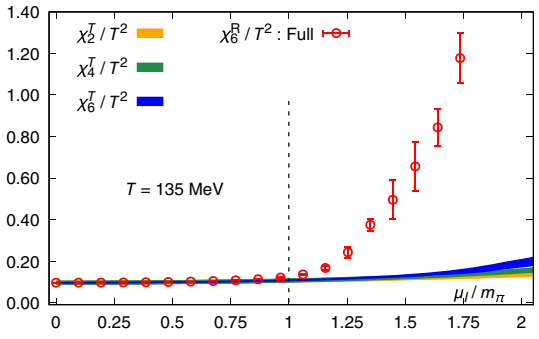


FIG. 5. Behavior of the number-density–to–isospin-chemical-potential ratio, i.e., isospin susceptibility χ_I, as a function of μ_I for different-order Taylor series (in bands) and for the full reweighting by unbiased exponential resummation (red circular points). The dotted vertical line resembles the $\mu_I = m_\pi$ line.

VI. RADIUS OF CONVERGENCE

Having outlined the behavior of the real and imaginary parts of the closest Lee-Yang zero μ^0_I as functions of T, we outline the radius of convergence estimate provided by μ^0_I for various working T in this section. Besides presenting some comparative studies, we also attempt to obtain a possible critical point estimate of the pion condensate phase boundary in the isospin phase diagram via linear extrapolation, which we detail in this section.

A. Results: From linear extrapolation fits

In this subsection, we outline the following: (1) the radius of convergence μ^ρ_I as a function of temperature T and (2) a possible estimate of the critical point on the second-order critical pion phase boundary, which we aim to attain by means of a linear extrapolation of the $\mu^T_{I,i}$ data points as a function of T, shown in Fig. 4. As known from previous works, the radius of convergence of the Taylor expansion of free energy or, equivalently, the free energy per unit volume, i.e., pressure, can offer a reliable estimate of the critical point. This coincides with the distance of the nearest Lee-Yang zero of the partition function from the origin in the complex μ plane ($\mu = \mu_I$ here). As mentioned before, Fig. 6 illustrates the T dependence of the physical radius of convergence μ^ρ_I in units of energy (MeV), which very understandably manifests a monotonic reduction of μ^ρ_I with lowering T in the hadronic regime below $T_{cr} \sim 157$ MeV.

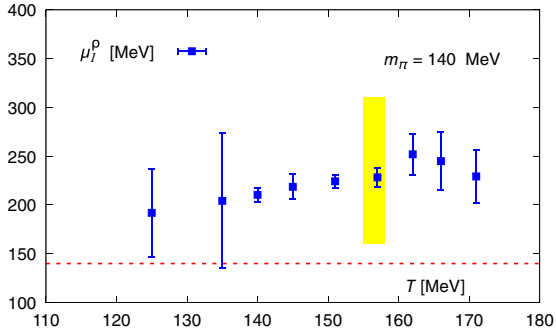


FIG. 6. Radius of convergence μ^ρ_I in units of MeV (blue points) as a function of temperature T, for $m_\pi = 140$ MeV.

In this figure, one also observes that, for low $T \leq 135$ MeV, these estimates come close to each other and agree within error bars with $\mu_I^\rho = 140$ MeV, shown by the red dotted line, which, as mentioned before, is the pion mass value used in this work. Unlike Ref. [39] which outlines a faster saturation of μ_I^ρ toward $\mu_I = 140$ MeV except for the choice of a different starting convention, the present observation in Fig. 6 yields a more gradual and monotonic nature in the decreasing values of μ_I^ρ with reducing values of T, which aligns better and is more consistent with the predictions of the χPT in [36]. These warrant further detailed work for obtaining enhanced definite conclusions.

For the critical point determination, we follow the usual state-of-the-art approach as followed before in numerous works involving Lee-Yang zeros [46–48]. The central idea is to evaluate the temperature T_I^c at which the nearest complex Lee-Yang zero becomes purely real and its imaginary part vanishes. With this value of T_I^c, we then procure the value of μ_I^c, which is $\mu_I^\rho(T)$ at $T = T_I^c$; subsequently, the physical critical point is given by (T_I^c, μ_I^c) in the $T - \mu_I$ plane. With no working data available at present for further lowering $T < 125$ MeV to outline the behavior of $\mu_{I,i}^T$ and μ_I^ρ for lower T, where one expects the former to vanish for some finite value of $T = T_I^c$, we resort to performing a linear extrapolation to these data points as shown in Figs. 4 and 6, respectively. This is also based on the observations from these figures, manifesting the monotonic behavior of $\mu_{I,i}^T$ and μ_I^ρ vs T in the hadronic regime. Despite having no notion of crossover in this probing regime of T and μ_I as per the current state-of-the-art isospin phase diagram, the extrapolation shown in Fig. 7 is carried out entirely with the purpose of determining an estimate of the critical temperature T_I^c within the present setup and limitations of this work. Without intending to locate the T_I^c in the thermodynamic limit, which we leave for a promising work in the future involving detailed volume dependence studies of these zeros, the extrapolation here rather attempts to illustrate the temperature-dependent trend in the behavior of these leading zeros and, by following this trend, to determine T_I^c at which the Lee-Yang zero becomes real with vanishing $\mu_{I,i}^0$.

We demonstrate the fit results explicitly in Fig. 7 where we consider, as input data to the fitting, only the blue data points lying in the low T hadronic regime below $T_{cr} \sim 157$ MeV (yellow band). The data points in the plasma regime for $T > T_{cr}$ outlined in brown are excluded and not considered for the linear fitting and extrapolation. Using linear *Ansätze* of the forms $\mu_{I,i}^T = aT + b$ and $\mu_I^\rho = cT + d$ with fitting parameters a, b, c, d, we employ error propagation and the least χ^2 fitting method and obtain the following estimates in MeV units:

$$T_I^c = 77.38 \pm 18.71,$$
$$\mu_I^c = 132.40 \pm 25.94. \tag{8}$$

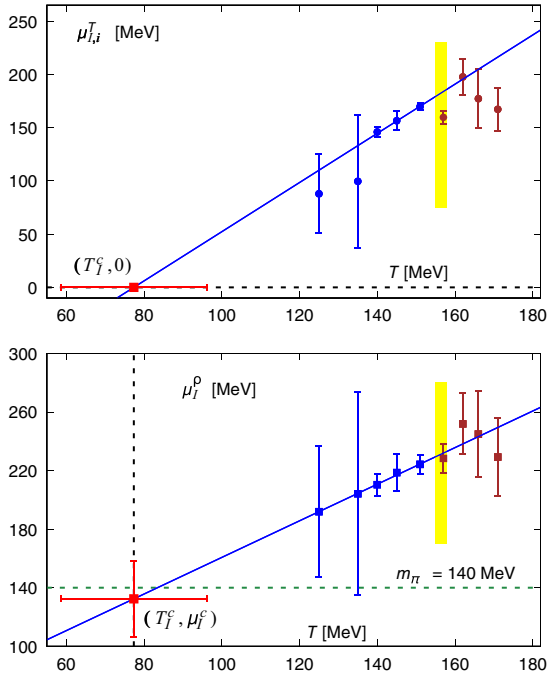


FIG. 7. Linear fitting and extrapolation to the data points concerning (top) $\mu_{I,i}^T$ and (bottom) μ_I^ρ. The horizontal and vertical error bars (in red) illustrate the errors in T_I^c and μ_I^c, respectively. See text for other details.

From the above calculation, we find small values of χ^2/d.o.f. around 0.7 and 0.02 for T_I^c and μ_I^c, respectively, which are possibly due to the large error bars for $T = 125$ and 135 MeV in Figs. 4 and 6. The larger errors for these temperatures also contribute to sizable errors in the respective T_I^c and μ_I^c estimates and thus require more attention. In this regard, future work may involve a higher number of statistics as well as bootstrap samples N_B. One can also attempt to work with further higher orders of unbiased resummation, which can possibly allow us to control these errors in a better fashion by eliminating higher-order biased contributions in μ_I.

Nevertheless, the present estimate (T_I^c, μ_I^c) in Eq. (8) of a possible critical point obtained, for the first time, using the unbiased exponential resummation method agrees commendably well within the respective error bars with the predicted second-order pion condensation phase boundary; at this lower $T \approx 80$ MeV, this should correspond to $\mu_I = m_\pi$ in the isospin phase diagram in the T-μ_I plane where m_π is equal to approximately 140 MeV, given this work is performed considering physical values of up and down (u, d) light quark masses in $(2+1)$-flavor QCD. The current stature of the pion condensate critical line, including its existence for low T, μ_I and its onset from $\mu_I = m_\pi$ at least for $T \leq 140$ MeV with the present working convention, is unanimously supported by present state-of-the-art works [38–40]. A positive feature of this estimate is that it is obtained from a direct Lee-Yang zero analysis of the isospin partition function without the requirement of

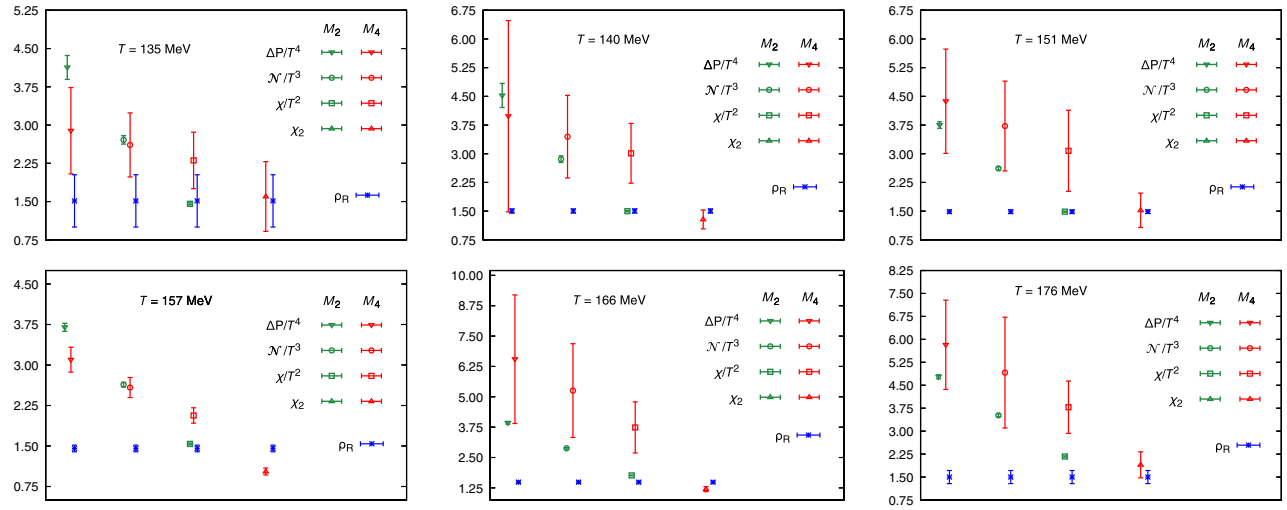


FIG. 8. Mercer-Roberts estimates $\mathcal{M}_n$ for $n = 2, 4$ obtained from the Taylor series of the first four cumulants ΔP, $\mathcal{N}$, χ, χ_2 for different $135 \leq T \leq 176$ MeV, shown by the green and red points. The blue points indicate the resummed estimate ρ_{R}.

calculating cumulants and their subsequent Lee-Yang singularities as done in some previous works [75,76]. Another positive achievement is that this result is attained naturally as an outcome of the simple linear extrapolation in this work without the need for any other *Ansätze* that relies on an *a priori* assumption about the properties of this pion condensation phase—such as its order, universality class, and point of onset in the isospin phase diagram—as possible input to the associated relevant fitting parameters and the fitting itself. This is significant and promising, despite the fact that this work, in its present form, does not infer anything about the order and universality class of this phase transition. Note that the visible discrepancy between our obtained T_I^c estimate in Eq. (8) and the same in [39] is because of different possible corrections contributed by the finite-volume effects of our working lattice, as well as the artifacts of the working method, which also cause finite $\mu_{I,i}^0$ values for $T \leq 140$ MeV as seen in Fig. 4 and clarified in Sec. V. To resolve these issues and understand their severity, one clearly requires simulations at higher lattice volumes, and one needs to explore the volume dependence of the respective $\mu_{I,r}^0, \mu_{I,i}^0$ of these zeros, by approaching the thermodynamic limit. As per the existing literature [39,73], one expects to observe real zeros with vanishing $\mu_{I,i}^0$ for all $T \leq 140$ MeV, and this is something we look to investigate thoroughly in a future work, as previously mentioned. In spite of these existing limitations to be further explored in the future, the positive upshot of this work is the successful mapping of a genuine critical point [Eq. (8)] on the second-order pion condensate critical line in the isospin phase diagram, using this Lee-Yang zero analysis.

Having the resummed estimate μ_I^ρ of the radius of convergence, we are now in a position to illustrate some comparisons, which we do in the following sections.

B. Comparisons with Mercer-Roberts estimates

In this section, we compare this resummed estimate of the dimensionless radius of convergence $\rho_{\mathrm{R}} = \mu_I^\rho/T$ with the MR estimates of the Taylor series. In relation to the Taylor series, this is important for determining the extent of reliability of this series approximation of the cumulant measurements in μ_I. Given the Taylor coefficients $c_n = \mathcal{X}_n/n!$, the nth order estimator for the MR method of estimation is given by

$$M_n = \left| \frac{c_{2n+2}c_{2n-2} - c_{2n}^2}{c_{2n+4}c_{2n} - c_{2n+2}^2} \right|^{1/2}, \tag{9}$$

where the different-order estimates converge to the true radius of convergence ρ in the $n \to \infty$ limit. We outline this comparison in Fig. 8, where we show the resummed radius of convergence ρ_R and the Mercer-Roberts estimates M_n for different orders n using the results of the Taylor coefficients c_n derived from the first three cumulants of the partition function, which are excess pressure ΔP, number density $\mathcal{N}$, and susceptibility χ. An important aspect to note in this regard is that the familiar ratio estimates ρ_n [77] of different orders n are not considered here for comparison. This is because they do not converge for the $n \to \infty$ limit, owing to the non-vanishing, finite imaginary parts of the leading complex Lee-Yang zeros for these temperatures. This feature has been detailed mathematically in [53]. In addition, previous studies [51,52] have showed that the Mercer-Roberts estimates exude better order-by-order stability, with more reliable convergent properties over the conventional ratio estimates ρ_n.

For these reasons, we only compare the resummed results with the different-order Mercer-Roberts estimates M_n for $n = 2, 4$ as given in Eq. (9). This comparison is

illustrated in Fig. 8. For M_4, we also highlight the fourth-order cumulant χ_2 defined as

$$\chi_2 = \left.\frac{\partial^2(\chi/T^2)}{\partial(\mu_I/T)^2}\right|_{\mu_I=0}.$$

The results are shown in Fig. 8. The more reliable M_4 out of the two estimates are shown by the red points in this figure. Like before, we observe that M_2 and M_4 reduce monotonically with an increasing order of cumulants. The larger error bars in M_4 are obvious because of the presence of less-precise higher-order Taylor coefficients c_6 and c_8. Nevertheless, within error bars, we find that both M_2 and M_4 approach the resummed results with an increasing order of the partition function cumulants. Because of some disagreement at the level of the third cumulant χ/T^2, we construct a fourth one, χ_2, which has been defined before. With this new cumulant, we observe agreement to a better extent between M_4 and the resummed $\rho_{\rm R}$ estimate. Despite still having some discrepancies at 157 and 166 MeV, the overall agreement achieved within errors for all the other working temperatures in Fig. 8 is encouraging. This highlights the utility of adopting this resummation approach and thereby using it to determine Lee-Yang zeros and the subsequent estimate of the radius of convergence, which we find can often indicate the same for the higher-order Taylor series expansion of higher-order cumulants of the QCD partition function.

C. Comparison among different-order cumulants of the isospin partition function

We extend this comparative discussion to the level of individual cumulants by highlighting the Taylor and unbiased exponential resummed results of the first three cumulants. We present this comparison for three temperatures, namely, 135, 157, and 166 MeV, in Fig. 9, where we also demonstrate these results as a function of real and imaginary μ_I values on the same plots.

We perform the unbiased exponential resummation series of these cumulants to second and fourth orders in real and imaginary μ_I, whereas the familiar and already-published Taylor series results are extracted up to eighth order. The resummed $\rho_{\rm R}$ estimates are depicted by the green bands in the figure. For all three cumulants in Fig. 9, we clearly observe that the lower second-order Taylor series results, shown by the blue points, diverge more quickly than the higher-order results, for both real and imaginary μ_I. As already proven in our previous paper [35], we observe and re-establish that the lower order resummed results agree appreciably well with similar and higher-order Taylor series results. However, the upshot and important observation in this case is that the agreement is sustained until

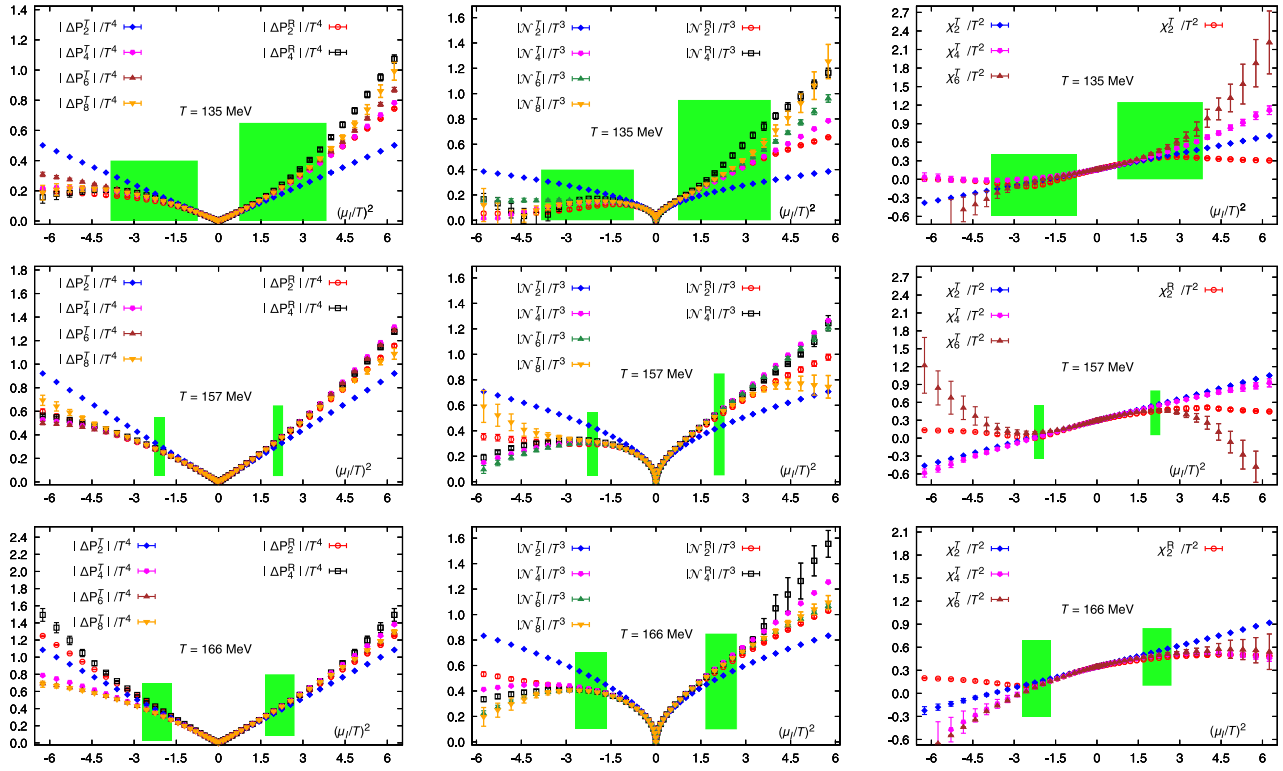


FIG. 9. Taylor and unbiased resummed results for the first three cumulants ΔP (left column), $\mathcal{N}$ (middle column), and χ (right column) for real and imaginary values of μ_I for $T = 135$ (top row), 157 (middle row), and 166 MeV (bottom row), respectively. The green bands show the resummed estimate $\rho_{\rm R}$ in the real and imaginary μ_I regimes.

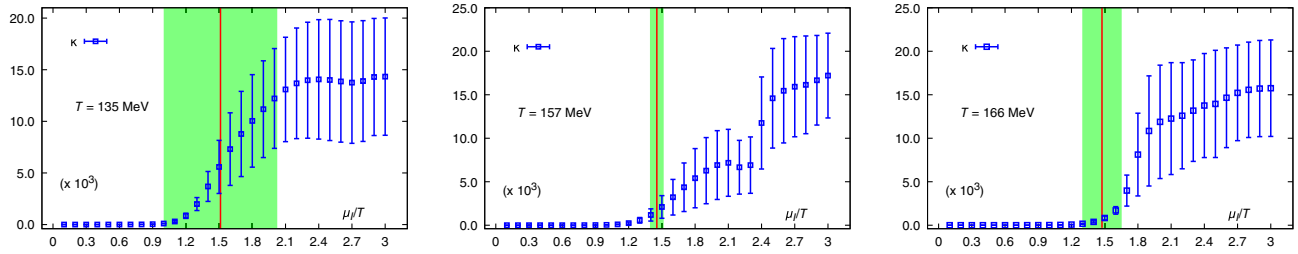


FIG. 10. Kurtosis κ as a function of real μ_I for 135 (left), 157 (middle), and 166 MeV (right), respectively. The red line shows the mean value of ρ_{R}, and the green band shows the same, along with the associated errors.

encountering the green bands, which depict the resummed estimate ρ_{R}, in Fig. 9. Beyond this estimate, i.e., for $|\mu_I| > \rho_{\mathrm{R}}$, we find that the different-order calculations of the resummed and Taylor series not only diverge away from one another but also, importantly, start manifesting the loss of monotonic behavior, which, otherwise as we observe, remains present for $|\mu_I| \leq \rho_{\mathrm{R}}$. In this regard, we also observe from Fig. 9 that the order-by-order departure and lack of monotonicity become increasingly more distinct and seemingly more precise with an increasing order of the cumulants.

VII. OVERLAP PROBLEM AND RESULTS

We provide a brief review of the overlap problem in this section. This problem, as well as its degree of severity for finite μ_I simulations, is important to understand the extent of reliability of using zero μ_I gauge ensembles in finite μ_I simulations. While calculations for finite μ_I do not possess a sign problem, one always needs to exercise caution regarding the ever-present overlap problem. This is because the degree of extrapolation to finite μ_I from $\mu_I = 0$ loses its reliability and efficacy once there is no significant overlap between the distributions of the reweighting factors between the target ensemble at a given μ_I and the known simulated ensemble at zero μ_I. Thus, this overlap becomes insignificant for larger values of μ_I, leading to greater degree of severity of the overlap problem.

For a given gauge field configuration, the extent of overlap is quantified by $\det \mathcal{M}(\mu_I)/\det \mathcal{M}(0)$, an unbiased estimate of which is given by

$$\frac{\det \mathcal{M}(\mu_I, U)}{\det \mathcal{M}(0, U)} = \exp\left[\sum_{n=1}^{N} \left(\frac{\mu_I}{T}\right)^n \frac{\mathcal{C}_n(U)}{n!}\right] \tag{10}$$

where $\mathcal{C}_n$ follows from Eq. (3). A direct measurement of this problem can, however, be obtained from kurtosis κ of the distribution of the determinant ratio, as outlined in Eq. (10). This is the standardized fourth-order central moment defined as

$$\kappa = \frac{M_4(\mu_I)}{[\sigma(\mu_I)]^4} \tag{11}$$

where we have the fourth central moment M_4 and the standard deviation σ as a function of μ_I.

Figure 10 portrays the behavior of κ as a function of μ_I for the three working temperatures 135,157, and 166 MeV. The red line, situated in the middle of the green band, illustrates the mean value of ρ_{R}. As expected, we observe that kurtosis κ increases with increasing values of μ_I. More importantly, the error bars start increasing, too, in a monotonic manner with increasing μ_I, and across the green band, they exude a sudden, sharp increment. We also note the nonmonotonicity in κ and the error bars in the $|\mu_I| > \rho_{\mathrm{R}}$ regime. This very clearly reflects the well-known fact that, across ρ_{R} from which the Lee-Yang zeros start appearing in the complex μ_I plane, this extrapolation to finite μ_I from $\mu_I = 0$ fails, and therefore, working with a gauge ensemble simulated at $\mu_I = 0$ is not viable.

VIII. CONCLUSIONS AND OUTLOOK

In this paper, we have demonstrated the Lee-Yang zeros of the QCD partition function in the complex isospin chemical potential μ_I plane, following the approach of unbiased exponential resummation. Throughout this work, we have managed to determine a possible estimate [see Eq. (8)] of one critical point situated on the second-order pion phase critical line in the low T, small μ_I regime of the QCD isospin phase diagram. As already outlined in this paper, an important feature of this method is the procedure of estimating the zeros directly from the path-integral form of the partition function itself. Unlike some of the previously related works in this direction, the Lee-Yang zeros and the subsequent (T_I^c, μ_I^c) are determined here entirely without utilizing any form of subsequent cumulants at any stage of the calculation, and also without invoking any property of this phase transition in the form of its order, universality class, or point of onset.

We have explicitly demonstrated in Fig. 1 the various estimates of Lee-Yang zeros in the complex μ_I plane for a wide range of temperatures from 125 to 171 MeV, including the crossover $T = 157$ MeV. As mentioned before, this full estimation has been done by utilizing the familiar Newton-Raphson method on the polynomial form of the partition function, which we have obtained in

an approximate form here by using the recent unbiased exponential resummation approach. For our work, the Lee-Yang zeros closest to origin in this complex μ_I plane are relevant since they offer the estimate of the radius of convergence of the Taylor expansion of free energy at $\mu_I = 0$. As it marks the upper bound of validity in μ_I starting from $\mu_I = 0$ of possible Taylor expansions which entirely rely on extrapolations from $\mu_I = 0$ or other $\mu_I < m_\pi$ values belonging in the uncondensed phase, this radius of convergence is believed to indicate and possibly outline the second-order pion condensate critical line in the isospin phase diagram, at least for lower values of T, μ_I. This critical line therefore outlines the upper limit of this uncondensed nonpion phase. To draw meaningful results and implications from these nearest Lee-Yang zeros, we have also verified their stability in Sec. IV B by implementing the Newton-Raphson method on these zero estimates, treating them as the new initial guesses. This is essential in realizing the reliability of the zeros, which we have shown here explicitly, to be trustworthy and commendable in the sense that the Newton-Raphson algorithm can identify them successfully when using them as the corresponding initial guess values. This is what we consider reliable, at least within the current precision and goal of this work, and also given the relevant associated observables considered in this paper. This has been outlined thoroughly in Sec. IV B through Figs. 2 and 3.

We have illustrated that while the imaginary parts of these zeros monotonically decrease with decreasing T, the real parts fluctuate but still manifest a sort of saturating feature and behavior toward $\mu_I = m_\pi$ from $T \leq 135$ MeV, also considering the associated error bars. This bodes well in agreement with the conclusions of some previous works stating that, from $T = 140$ MeV, the pion phase boundary becomes vertical and, without too much thermal variation, converges to $\mu_I = m_\pi$ at zero T. Although the radius of convergence in Fig. 6 shows some discrepancy to this notion, presumably because of the finite imaginary part of the zeros, its behavior showcasing a monotonic reduction with decreasing T, at least in the hadronic regime, is consistent with the chiral perturbation theory implications which hold true in the $\mu_I < m_\rho$ regime of exploration, where $m_\rho = 770$ MeV. By means of a linear extrapolation, which we perform solely in the spirit of following the thermal trend of the Lee-Yang zeros without regard to the usual differentiation between the crossover and phase transitions, we have determined the possible estimate of a critical point, and we have demonstrate in Sec. VI A that this critical point is located at $\mu_I = m_\pi$, essentially within error bars around $T = 80$ MeV, which we show in Fig. 7, where observe that the imaginary part $\mu^0_{I,i}$ of the nearest Lee-Yang zero vanishes, consequently positioning it on the real μ_I axis. Even though this estimate of T^c_I is less than 140 MeV, the critical point thus obtained converges to a true one on the second-order critical line. The present study can be argued to provide a possible lower bound in the sense that the second-order pion condensate line can be predicted to exist at least for $T \in [0 : T^c_I]$ within error bars. As mentioned before, several further studies are expected, involving finite-size scaling analysis of these zeros and their behavior in the thermodynamic limit; these studies are expected to provide a better picture outlining possible reasons for this difference, besides manifesting real zeros for all $T \leq 140$ MeV, and thereby aligning with the present state-of-the-art QCD isospin phase diagram, at least in this regime. We consider all these crucial, important studies to be outside the scope of the current work and reserve them for interesting future work, with the belief that this will surely enlighten and establish further aspects of the phase diagram, especially in the low T regime, close to $T = 0$ from this approach. We also plan to approach the thermodynamic and continuum limits in the future and subsequently investigate the location of these zeros, with lower values of tolerance for the Newton-Raphson method. Nevertheless, the very observation of the linearly extrapolated radius of convergence merging to a possible valid critical point on the second-order pion phase boundary for $T = 80$ MeV is a novel feature of this work, given its present scope and limitations.

In Sec. VI B, we have outlined a detailed discussion of the resummed version ρ_R of the dimensionless radius of convergence by comparing it with the well-known Mercer-Roberts estimates of the same obtained via the Taylor series. This is illustrated by considering the series expansions of different-order cumulants, starting from excess pressure (zeroth cumulant) to the fourth cumulant χ_2. We have also extended our analysis to include comparisons between Taylor and unbiased exponential results in real and imaginary μ_I values for the first three cumulants of the QCD partition function, which we have illustrated in Fig. 9. These indicate that the results sustain order-by-order convergence within and up to ρ_R, beyond which they show a lack of monotonicity as well as divergences among different orders. Finally, in Sec. VII, we showed that the overlap problem becomes severely drastic starting from this radius of convergence. Indicated by the stark increment of kurtosis with a sudden rise in associated error bars, this reflects minimal overlap between the target and simulated distributions starting from this regime and due to which the zero μ_I extrapolation used fails and lacks reliability here. Overall, with the limitations and scope of further improvements, we have attempted to show that the unbiased exponential resummation approach can offer a reliable resummed estimate of the radius of convergence through Lee-Yang zero estimates, and this has the potential to locate one of the constituent critical points on the critical second-order pion phase boundary line in the QCD isospin phase diagram.

ACKNOWLEDGMENTS

I sincerely acknowledge Jishnu Goswami for useful discussions and suggestions for the draft. I also thank the other members of the HotQCD Collaboration for their valuable input as well as for allowing me to use their data for the respective Taylor expansion calculations. The computations in this work have been performed on the GPU cluster at Bielefeld University, Germany. I would also like to greatly thank the Bielefeld HPC.NRW team for their support.

DATA AVAILABILITY

The data that support the findings of this article are openly available [78].

APPENDIX: FIXING OUR CHOICE OF THE INITIAL CONVENTION OF ISOSPIN

For setting up the relations between the chemical potentials of the u, d, s basis and our working B, S, I basis in this work, we have considered the usual quantum number relations in $(2+1)$-flavor QCD as follows:

$$B=\frac{1}{3}(N_u+N_d), \quad S=-N_s, \quad I=\frac{1}{2}(N_u-N_d). \tag{A1}$$

Here B, S, I stands for baryon, strangeness, and isospin quantum numbers, respectively, with N_u, N_d, N_s being the number of up, down, and strange quarks.

The isospin prefactor $1/2$ in Eq. (A1) comes from the fact that protons and neutrons have isospin $1/2$ since one can be formed from the other by interchanging an up quark with a down quark and vice versa. In addition, since they are baryons and therefore three-quark spin $1/2$ systems, the constituent up and down quarks should also have isospin quantum numbers $1/2$. The assignment of $+1/2$ to protons and u quarks and $-1/2$ to neutrons and d quarks depends on one's choice. This motivates us to choose each u quark to have $I_u = 1/2$ and each d quark to have $I_d = -1/2$. Since the property of strangeness comes entirely from the strange quark, we assign $I_s = -1$ to the strange quark. This logically leads us to Eq. (A1). With this, naturally, the pion quantum number $I_\pi = 1$, as it is a two quark system (meson) and it comes in three species π^+, π^-, π^0. This can also be justified using the familiar quantum-mechanical relation $N_I = 2I + 1$. In this case, $I = 1$ for the pion, and hence, the number of possible pions is $N_I = 3$.

With the set of equations in (A1) and also the fugacity conservation equation $\mu_B B + \mu_S S + \mu_I I = \mu_u N_u + \mu_d N_d + \mu_s N_s$, we therefore find

$$\mu_B = \frac{3}{2}(\mu_u + \mu_d), \qquad \mu_I = (\mu_u - \mu_d), \tag{A2}$$

where μ_B, μ_I are the baryon and isospin chemical potentials and μ_u, μ_d are the same for up and down quarks, respectively. This is precisely the starting convention used in this work and also in a recent work [79].

[1] E. V. Shuryak, Quark-gluon plasma and hadronic production of leptons, photons and psions, Phys. Lett. **78B**, 150 (1978).
[2] K. Aamodt *et al.* (ALICE Collaboration), The ALICE experiment at the CERN LHC, J. Instrum. **3**, S08002 (2008).
[3] M. Gyulassy and L. McLerran, New forms of QCD matter discovered at RHIC, Nucl. Phys. **A750**, 30 (2005).
[4] K. Adcox *et al.* (PHENIX Collaboration), Formation of dense partonic matter in relativistic nucleus-nucleus collisions at RHIC: Experimental evaluation by the PHENIX Collaboration, Nucl. Phys. **A757**, 184 (2005).
[5] G. Aad *et al.*, The ATLAS experiment at the CERN Large Hadron Collider, J. Instrum. **3**, S08003 (2008).
[6] W. Busza, K. Rajagopal, and W. V. Schee, Heavy ion collisions: The big picture, and the big questions, Annu. Rev. Nucl. Part. Sci. **68**, 339 (2018).
[7] C. Ratti, Lattice QCD and heavy ion collisions: A review of recent progress, Rep. Prog. Phys. **81**, 084301 (2018).
[8] G. Baym, H. A. Bethe, and C. Pethick, Neutron star matter, Nucl. Phys. **A175**, 225 (1971).
[9] E. V. Shuryak, Quantum chromodynamics and the theory of superdense matter, Phys. Rep. **61**, 71 (1980).
[10] G. Baym, T. Hatsuda, T. Kojo, P. D. Powell, Y. Song, and T. Takatsuka, From hadrons to quarks in neutron stars: A review, Rep. Prog. Phys. **81**, 056902 (2018).
[11] S. Barshay, G. Vagradov, and G. E. Brown, Possibility of a phase transition to a pion condensate in neutron stars, Phys. Lett. **43B**, 359 (1973).
[12] E. W. Kolb, *The Early Universe* (Taylor and Francis, London, 2019), Vol. 69, ISBN: 978-0-429-49286-0, 978-0-201-62674-2.
[13] A. M. Halasz, A. D. Jackson, R. E. Shrock, M. A. Stephanov, and J. J. M. Verbaarschot, On the phase diagram of QCD, Phys. Rev. D **58**, 096007 (1998).
[14] F. Karsch, Lattice QCD at high temperature and density, Lect. Notes Phys. **583**, 209 (2002).
[15] A. Bazavov *et al.* (HotQCD Collaboration), Equation of state in $(2+1)$-flavor QCD, Phys. Rev. D **90**, 094503 (2014).
[16] A. Bazavov *et al.* (HotQCD Collaboration), Chiral crossover in QCD at zero and non-zero chemical potentials, Phys. Lett. B **795**, 15 (2019).

[17] P. Steinbrecher, The QCD crossover at zero and non-zero baryon densities from lattice QCD, Nucl. Phys. **A982**, 847 (2019).
[18] S. Borsanyi *et al.*, QCD crossover at finite chemical potential from lattice simulations, Phys. Rev. Lett. **125**, 052001 (2020).
[19] F. Karsch and K. H. Mutter, Strong coupling QCD at finite baryon number density, Nucl. Phys. **B313**, 541 (1989).
[20] F. Karsch, Lattice QCD at finite temperature and density, Nucl. Phys. B, Proc. Suppl. **83**, 14 (2000).
[21] P. Forcrand, Simulating QCD at finite density, Proc. Sci. LAT2009 (**2009**) 010 [arXiv:1005.0539].
[22] W. J. Fu, J. M. Pawlowski, and F. Rennecke, QCD phase structure at finite temperature and density, Phys. Rev. D **101**, 054032 (2020).
[23] Z. Fodor and S. D. Katz, Lattice determination of the critical point of QCD at finite T and mu, J. High Energy Phys. 03 (2002) 014.
[24] F. Karsch, E. Laermann, and C. Schmidt, The chiral critical point in three-flavor QCD, Phys. Lett. B **520**, 41 (2001).
[25] R. V. Gavai and S. Gupta, The critical end point of QCD, Phys. Rev. D **71**, 114014 (2005).
[26] I. Barbour, N. E. Behilil, E. Dagotto, F. Karsch, A. Moreo, M. Stone, and H. W. Wyld, Problems with finite density simulations of lattice QCD, Nucl. Phys. **B275**, 296 (1986).
[27] Z. Fodor and S. D. Katz, A new method to study lattice QCD at finite temperature and chemical potential, Phys. Lett. B **534**, 87 (2002).
[28] G. Pan and Z. Y. Meng, Sign problem in quantum Monte Carlo simulation, Encycl. Condens. Matter Phys. **1**, 879 (2024).
[29] R. V. Gavai and S. Gupta, The critical end point of QCD, Phys. Rev. D **71**, 114014 (2005).
[30] P. de Forcrand and O. Philipsen, QCD phase diagram at small densities from simulations with imaginary μ, in *5th International Conference on Strong and Electroweak Matter* (2003), pp. 271–275, arXiv:hep-ph/0301209.
[31] A. Alexandru, G. Basar, and P. Bedaque, Monte Carlo algorithm for simulating fermions on Lefschetz thimbles, Phys. Rev. D **93**, 014504 (2016).
[32] D. Sexty, Simulating full QCD at nonzero density using the complex Langevin equation, Phys. Lett. B **729**, 108 (2014).
[33] S. Mondal, S. Mukherjee, and P. Hegde, Lattice QCD equation of state for nonvanishing chemical potential by resumming Taylor expansions, Phys. Rev. Lett. **128**, 022001 (2022).
[34] D. Bollweg *et al.*, Taylor expansions and Padé approximants for cumulants of conserved charge fluctuations at nonvanishing chemical potentials, Phys. Rev. D **105**, 074511 (2022).
[35] S. Mitra and P. Hegde, QCD equation of state at finite chemical potential from an unbiased exponential resummation of the lattice QCD Taylor series, Phys. Rev. D **108**, 034502 (2023).
[36] D. T. Son and M. A. Stephanov, QCD at finite isospin density, Phys. Rev. Lett. **86**, 592 (2001).
[37] P. Forcrand, M. A. Stephanov, and U. Wenger, On the phase diagram of QCD at finite isospin density, Proc. Sci. LATTICE2007 (**2007**) 237 [arXiv:0711.0023].
[38] J. O. Andersen, M. Johnsrud, Q. Yu, and H. Zhou, Chiral perturbation theory and Bose-Einstein condensation in QCD, Phys. Rev. D **111**, 034017 (2025).
[39] B. B. Brandt, G. Endrodi, and S. Schmalzbauer, QCD phase diagram for nonzero isospin-asymmetry, Phys. Rev. D **97**, 054514 (2018).
[40] B. B. Brandt, F. Cuteri, G. Endrodi, and S. Schmalzbauer, Exploring the QCD phase diagram via reweighting from isospin chemical potential, Proc. Sci. LATTICE2019 (**2019**) 189.
[41] T. Yokota *et al.*, Color superconductivity on the lattice—analytic predictions from QCD in a small box, J. High Energy Phys. 06 (2023) 061.
[42] U. Reinosa, J. Serreau, and M. Tissier, Perturbative study of the QCD phase diagram for heavy quarks at nonzero chemical potential, Phys. Rev. D **92**, 025021 (2015).
[43] S. Scherer, Introduction to chiral perturbation theory, Adv. Nucl. Phys. **27**, 277 (2003).
[44] A. Alexandru, M. Faber, I. Horváth, and K. F. Liu, Lattice QCD at finite density via a new canonical approach, Phys. Rev. D **72**, 114513 (2005).
[45] S. Mitra, Exponential resummation of QCD at finite chemical potential, Ph.D. thesis, Indian Institute of Science Bangalore, Centre for High Energy Physics, India, 2023, arXiv:2307.05751.
[46] P. Dimopoulos *et al.*, Contribution to understanding the phase structure of strong interaction matter: Lee-Yang edge singularities from lattice QCD, Phys. Rev. D **105**, 034513 (2022).
[47] C. Schmidt *et al.*, Detecting critical points from the Lee–Yang edge singularities in lattice QCD, Acta Phys. Pol. B Proc. Suppl. **16**, 1 (2023).
[48] D. A. Clarke *et al.*, Searching for the QCD critical point using Lee-Yang edge singularities, Proc. Sci. LATTICE2023 (**2024**) 168 [arXiv:2401.08820].
[49] D. A. Clarke *et al.*, Searching for the QCD critical endpoint using multi-point Padé approximations, arXiv:2405.10196.
[50] T. D. Lee and C. N. Yang, Statistical theory of equations of state and phase transitions. II. Lattice gas and Ising model, Phys. Rev. **87**, 410 (1952).
[51] G. N. Mercer and A. J. Roberts, A centre manifold description of contaminant dispersion in channels with varying flow properties, SIAM J. Appl. Math. **50**, 1547 (1990).
[52] V. VovchenkoJ. Steinheimer, O. Philipsen, and H. Stoecker, Cluster expansion model for QCD baryon number fluctuations: No phase transition at $\mu_B/T < \pi$, Phys. Rev. D **97**, 114030 (2018).
[53] M. Giordano and A. Pásztor, Reliable estimation of the radius of convergence in finite density QCD, Phys. Rev. D **99**, 114510 (2019).
[54] R. Gavai, S. Gupta, and R. Ray, Taylor expansions in chemical potential, Prog. Theor. Phys. Suppl. **153**, 270 (2004).
[55] S. Ejiri *et al.*, Study of QCD thermodynamics at finite density by Taylor expansion, Prog. Theor. Phys. Suppl. **153**, 118 (2004).
[56] C. Miao and C. Schmidt, Non-zero density QCD by the Taylor expansion method: The isentropic equation of state, hadronic fluctuations and more, Proc. Sci. LATTICE2008 (**2008**) 172 [arXiv:0810.0375].

[57] F. Karsch, B.-J. Schaefer, M. Wagner, and J. Wambach, Towards finite density QCD with Taylor expansions, Phys. Lett. B **698**, 256 (2011).
[58] D. Bollweg, J. Goswami, O. Kaczmarek, F. Karsch, S. Mukherjee, P. Petreczky, C. Schmidt, and P. Scior, Taylor expansions and Padé approximants for cumulants of conserved charge fluctuations at nonvanishing chemical potentials, Phys. Rev. D **105**, 074511 (2022).
[59] K. Symanzik, Continuum limit and improved action in lattice theories. 1. Principles and φ^4 theory, Nucl. Phys. **B226**, 187 (1983).
[60] E. Follana *et al.* (HPQCD and UKQCD Collaborations), Highly improved staggered quarks on the lattice, with applications to charm physics, Phys. Rev. D **75**, 054502 (2007).
[61] A. Bazavov and P. Petreczky, Deconfinement and chiral transition with the highly improved staggered quark (HISQ) action, J. Phys. Conf. Ser. **230**, 012014 (2010).
[62] A. Bazavov *et al.*, The chiral and deconfinement aspects of the QCD transition, Phys. Rev. D **85**, 054503 (2012).
[63] S. Mitra, P. Hegde, and C. Schmidt, New way to resum the lattice QCD Taylor series equation of state at finite chemical potential, Phys. Rev. D **106**, 034504 (2022).
[64] S. Mitra, Determination of lattice QCD equation of state at a finite chemical potential, Springer Proc. Phys. **304**, 209 (2024).
[65] S. Mitra, P. Hegde, and C. Schmidt, A new way to resum Lattice QCD equation of state at finite chemical potential, Proc. Sci. LATTICE2022 (**2023**) 153 [arXiv:2209.07241].
[66] T. J. Ypma, Historical development of the Newton–Raphson method, SIAM Rev. **37**, 531 (1995).
[67] A. Bazavov *et al.*, The QCD equation of state to $\mathcal{O}(\mu_B^6)$ from lattice QCD, Phys. Rev. D **95**, 054504 (2017).
[68] A. Bazavov *et al.*, Chiral crossover in QCD at zero and non-zero chemical potentials, Phys. Lett. B **795**, 15 (2019).
[69] D. Bollweg *et al.*, Second order cumulants of conserved charge fluctuations revisited: Vanishing chemical potentials, Phys. Rev. D **104**, 074512 (2021).
[70] D. Bollweg *et al.*, Taylor expansions and Padé approximants for cumulants of conserved charge fluctuations at nonvanishing chemical potentials, Phys. Rev. D **105**, 074511 (2022).
[71] D. Bollweg *et al.*, Equation of state and speed of sound of $(2+1)$-flavor QCD in strangeness-neutral matter at nonvanishing net baryon-number density, Phys. Rev. D **108**, 014510 (2023).
[72] Z. Fodor and S. D. Katz, Lattice QCD thermodynamics, Acta Phys. Pol. B **42**, 2791 (2011).
[73] S. Borsanyi, Z. Fodor, M. Giordano, J. N. Guenther, S. D. Katz, A. Pasztor, and C. H. Wong, Can rooted staggered fermions describe nonzero baryon density at low temperatures?, Phys. Rev. D **109**, 054509 (2024).
[74] Rho meson mass $m_\rho = 770$ MeV.
[75] C. Schmidt, Lee-Yang edge singularities in QCD: From Fourier coefficients to parametrizations of the universal scaling functions, Proc. Sci. EuroPLEx2023(**2024**) 037.
[76] C. Schmidt, The QCD phase diagram, universal scaling, and Lee-Yang zeros, J. Subatomic Part. Cosmol. **3**, 100057 (2025).
[77] $\rho_n = \sqrt{c_{2n}/c_{2n+2}}$.
[78] S. Mitra, PUB–Publikationen an der Universität Bielefeld (2025), 10.4119/unibi/3004966.
[79] J. O. Andersen, Q. Yu, and H. Zhou, Pion condensation in QCD at finite isospin density, the dilute Bose gas, and speedy Goldstone bosons, Phys. Rev. D **109**, 034022 (2024).